Some Flutter Solutions Using Finite Elements

MERVYN D. OLSON*
National Aeronautical Establishment, Ottawa, Canada

The application of the finite-element method to supersonic flutter problems is presented. Two rectangular plate bending elements (the 12-parameter nonconforming model and the 16-parameter conforming one) and an 18-parameter conforming triangular element are used. Two-dimensional, quasi-steady aerodynamic matrices are derived for these elements from virtual work principles. The flutter of a square, simply supported panel is analyzed with various assemblages of both rectangular elements. A comparison with the exact solution indicates that the conforming element yields superior results. These latter elements are then used to analyze a square clamped panel, a problem for which no exact solution is available. The triangular finite elements are applied to the flutter of several cantilevered delta wings. The calculations compare well with experimental results available in the literature even for quite low aspect ratio configurations.

Nomenclature

a,b	=	rectangular element dimensions, Fig. 1
a_∞	=	freestream speed of sound
$[A_e],[A]$	=	aerodynamic matrices for finite element and total structure, respectively
c	=	semichord of delta wings
D	=	plate bending rigidity
g_a	=	aerodynamic damping parameter, Eq. (15)
h	=	plate thickness
$k;k_{cr}$	=	eigenvalue, Eq. (13); coalescence value
k_R,k_I	=	real and imaginary parts of k
$[K_e],[K]$	=	stiffness matrices for finite element and total structure, respectively
L	=	length of plate or wing
M_∞	=	Mach number
$[M_e],[M]$	=	mass matrices for finite element and total structure, respectively
n	=	number of elements per side of plate
q	=	dynamic pressure
U	=	freestream velocity
w,η	=	plate deflections, Eq. (2)
w_x,w_{xy}	=	$\partial w/\partial x$, $\partial^2 w/\partial x\partial y$, etc.
λ,λ_{cr}	=	nondimensional dynamic pressure $= 2qL^3/D(M_\infty^2-1)^{1/2}$ and coalescence value, respectively
μ	=	mass density parameter, Ref. (12)
Λ	=	sweepback angle of delta wings
ν	=	coefficient of time dependence, Eq. (2)
ρ,ρ_a	=	plate material and air density, respectively
ω	=	circular frequency
ω_0	=	frequency scale $= (D/\rho hL^4)^{1/2}$
ω_α	=	second natural frequency for delta wing

1. Introduction

IN the past few years, considerable progress has been made in developing finite-element techniques for structural analysis. The finite-element method is being extended to almost all branches of solid mechanics, and problems are being tackled which were previously considered unsolvable. Almost all types of plate and shell problems encountered in the aerospace field are currently being analyzed. Some of the latest extensions include wave propagation, random response, buckling, geometric nonlinearities and elastic-plastic analysis.

Presented at the AIAA Structural Dynamics and Aeroelasticity Specialist Conference, New Orleans, La., April 16–17, 1969; submitted April 29, 1969; revision received September 2, 1969.

* Assistant Research Officer, Structures and Materials Laboratory. Member AIAA.

It appears that aeroelasticians are just beginning to recognize the potential of the method for their work. However, many current flutter calculations still depend on experimentally measured mode shapes and/or influence coefficients or, at best, estimates of these from crude theories. With finite-element techniques, it is becoming possible to eliminate these limitations. Either the method may be used to predict more accurate mode shapes required for a modal analysis or the flutter calculations may be carried out directly, thus avoiding the modal analysis completely. This latter approach takes advantage of the full potential of the method and is the one adopted in the following.

The finite-element method was first applied to two-dimensional panel flutter by the author.[1] There it was shown that only a few elements were required to yield completely satisfactory results. In the present paper, the method is extended to three-dimensional applications using both rectangular and triangular plate bending elements. The present applications are restricted to the supersonic range, and two-dimensional, quasi-static aerodynamic theory is assumed accurate enough for the limited trend studies to be presented herein. Although the use of this aerodynamic theory for three-dimensional applications may sound inconsistent, past experience has shown that it yields surprisingly good results even for quite low aspect ratio configurations. The quasi-static assumption limits the applications to cases with low reduced frequencies. Consistent aerodynamic matrices are derived for all three elements from virtual work principles.

The rectangular plate bending elements employed here are the well-known 12-parameter nonconforming model[2] and the newer, 16-parameter conforming model developed by Bogner, Fox and Schmit.[3] The former element provides only displacement continuity between adjacent elements, whereas the latter one provides slope continuity as well. Hence, monotonic convergence of the total potential energy in static problems is guaranteed only when using the latter elements. The flutter of a simply supported square panel is analyzed with various assemblages of both these elements, and the results are compared with the exact solution. It is found that the conforming element gives the best results, and hence is used to analyze the flutter of a clamped square panel, a previously unsolved problem.

A triangular plate bending element is used in the final part of the study, so that problems with nonrectangular boundaries may be analyzed. The element chosen is a new 18-degree-of-freedom model[4–6] which outperforms all previously available representations. Six parameters, w, $\partial w/\partial x$, $\partial w/\partial y$, $\partial^2 w/\partial x^2$, $\partial^2 w/\partial x\partial y$, and $\partial^2 w/\partial y^2$, are used at each corner of

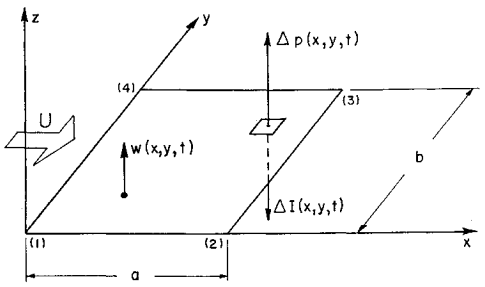

Fig. 1 Rectangular finite plate element.

this element and provide complete displacement and slope continuity between adjacent elements. Calculations are carried out for cantilevered wings of delta planform with various assemblages of the triangular elements, and the results are compared with experimental results available in the literature.

Since the present study was completed, some similar work has been reported by Kariappa and Somashekar.[7] However, they treat only the nonconforming rectangular element and present results from only one gridwork of these elements. Hence, it is very difficult to judge the accuracy of the method from their limited study.

2. Theoretical Formulation

Consider the rectangular finite element depicted in Fig. 1. For simplicity, it is assumed that the air flowing above the panel is parallel to the x-axis and that the effect of any air entrapped below may be neglected. Assuming two-dimensional supersonic aerodynamic theory is sufficiently accurate, the aerodynamic force acting on an infinitesimal element $dxdy$ is

$$\Delta p(x,y,t) = \frac{2q}{(M_\infty^2 - 1)^{1/2}}\left[\frac{\partial w}{\partial x} + \frac{1}{U}\frac{M_\infty^2 - 2}{M_\infty^2 - 1}\frac{\partial w}{\partial t}\right] dxdy \quad (1)$$

where q, M_∞ and U are the dynamic pressure, Mach number and flow velocity, respectively. Assuming exponential dependence on time

$$w(x,y,t) = \eta(x,y)e^{\nu t} \quad (2)$$

allows the aerodynamic force to be separated into

$$\Delta p = [\Delta P_a + \Delta P_d]e^{\nu t} \quad (3)$$

where

$$\Delta P_a = [2q/(M_\infty^2 - 1)^{1/2}](\partial\eta/\partial x)dxdy \quad (4)$$

and

$$\Delta P_d = (2q\nu/U)[M_\infty^2 - 2/(M_\infty^2 - 1)^{3/2}]\eta\, dxdy \quad (5)$$

It is clear that ΔP_a is the primary aerodynamic force, since it is proportional to the slope $\partial\eta/\partial x$, while ΔP_d is the aerodynamic damping and is proportional to the displacement η. Hence, ΔP_d may be combined with the usual inertia force

$$\Delta I(x,y,t) = \rho h\nu^2\eta dxdy \quad (6)$$

to yield an effective inertia force

$$\Delta I_e = \Delta I + \Delta P_d = \left[\rho h\nu^2 + \frac{2q\nu}{U}\frac{M_\infty^2 - 2}{(M_\infty^2 - 1)^{3/2}}\right]\eta dxdy \quad (7)$$

Therefore, the effect of the aerodynamic damping is readily included in the finite element method by replacing the usual inertia parameter $\rho h\nu^2$ with $\rho h\nu^2 + 2q\nu(M_\infty^2 - 2)/U(M_\infty^2 - 1)^{3/2}$.

To include the effect of the aerodynamic force of Eq. (4), it is necessary to derive an aerodynamic matrix. This is achieved through a calculation of virtual work. The virtual work of the aerodynamic force is

$$V_a = \iint\tilde{\eta}\Delta P_a = [2q/(M_\infty^2 - 1)^{1/2}]\iint\tilde{\eta}(\partial\eta/\partial x)dxdy \quad (8)$$

where $\tilde{\eta}$ is the virtual displacement, and the integration is over the area of the finite element. In the finite-element approximation, η is usually assumed in the form

$$\eta(x,y) = \{W\}^T\{f\} \quad (9)$$

where $\{W\}$ is a column vector of generalized displacements and $\{f\}$ is a column vector of interpolation functions in x and y. Particular examples of these vectors will be considered in the next section. Introducing Eq. (9) into Eq. (8) yields

$$V_a = \{\tilde{W}\}^T[A_e]\{W\} \quad (10)$$

where

$$[A_e] = [2q/(M_\infty^2 - 1)^{1/2}]\iint\{f\}^T\{\partial f/\partial x\}\, dxdy \quad (11)$$

is the required aerodynamic matrix for the particular finite element being considered.

The stiffness and mass matrices, $[K_e]$ and $[M_e]$, respectively, for the finite elements to be employed herein are available in the literature and hence are not presented here. Putting all the matrices together yields the equation for the generalized forces acting on a finite element as

$$\{F\} = [K_e + \alpha A_e - \delta M_e]\{W\} \quad (12)$$

where $\{F\}$ is a column vector of generalized forces corresponding to the generalized coordinates $\{W\}$. The total matrix enclosed by the outer square brackets represents the generalized aerodynamic-stiffness matrix for a finite element. Assembling the finite elements to approximate a particular structure then follows a fairly standard procedure. The master aerodynamic-stiffness matrix for the structure is obtained from an assemblage of the individual element matrices by equating corresponding generalized coordinates at corner junctions and equating the sums of corresponding generalized forces there to zero. The homogeneous kinematic boundary conditions are applied by striking out the appropriate rows and columns. This leads to a final eigenvalue problem of the form

$$[K + \lambda A - kM]\{W\} = 0 \quad (13)$$

where

$$\lambda = 2qL^3/D(M_\infty^2 - 1)^{1/2}$$

and

$$k = -\lambda(M_\infty^2 - 2)/(M_\infty^2 - 1)(L/U)\nu - (\rho hL^4/D)\nu^2$$

are the nondimensional dynamic pressure parameter and eigenvalue, respectively. The master aerodynamic matrix $[A]$ is nonsymmetric, and hence nonreal eigenvalues k are expected for $\lambda > 0$. For $\lambda = 0$ however, the eigenvalues are real and positive, since $[K]$ and $[M]$ are symmetric and positive definite. As λ is increased from zero, two of these eigenvalues will usually approach each other and coalesce to k_{cr} at $\lambda = \lambda_{cr}$ and become complex conjugate pairs

$$k = k_R \pm ik_I \quad (14)$$

for $\lambda > \lambda_{cr}$. Here λ_{cr} is considered to be that value of λ at which first coalescence occurs. The eigenvalue k may be put in the more convenient form

$$k = -g_a(\nu/\omega_0) - (\nu^2/\omega_0^2) \quad (15)$$

where

$$g_a = (M_\infty^2 - 2)\,\rho_a U/(M_\infty^2 - 1)^{3/2}\,\rho h\omega_0$$

is the nondimensional aerodynamic damping parameter. $\omega_0 = (D/\rho hL^4)^{1/2}$ is a convenient frequency scale that is re-

Table 1 Aerodynamic matrix 5040 $(M_\infty^2 - 1)^{1/2}[A_e]/2qa^2b$ for nonconforming rectangular element[a]

0	−21	−175	−28	21	175	−14	−14	77	0	14	−77
21	−24	−132	−21	24	132	−14	−18	78	14	18	−78
175	−132	−936	−175	132	936	−77	−78	324	77	78	−324
28	21	175	0	−21	−175	0	14	−77	14	−14	77
−21	−24	−132	21	24	132	14	−18	78	−14	18	−78
−175	−132	−936	175	132	936	77	−78	324	−77	78	−324
14	14	77	0	−14	−77	0	21	−175	28	−21	175
14	18	78	−14	−18	−78	−21	24	−132	21	−24	132
−77	−78	−324	77	78	324	175	−132	936	−175	132	−936
0	−14	−77	−14	14	77	−28	−21	175	0	21	−175
−14	18	78	14	−18	−78	21	24	−132	−21	−24	132
77	−78	−324	−77	78	324	−175	−132	936	175	132	−936

[a] Rows and columns 2, 5, 8, and 11 are to be divided by $s = a/b$.

lated to the first natural frequency for a semi-infinite simply supported panel.

Now for steady state flutter, $\nu = i\omega$, and combining Eqs. (14) and (15) yields the flutter frequency and aerodynamic damping

$$\omega/\omega_0 = (k_R)^{1/2},\ g_a = k_I/(k_R)^{1/2} \tag{16}$$

Hence, the flutter boundary as a function of the aerodynamic damping g_a may be obtained by continuing the calculations for $\lambda > \lambda_{cr}$. It is worth noting here that this procedure is different from the one put forward in Ref. 7, where the aerodynamic damping was introduced as a complex quantity in the master matrix, Eq. (13). The present procedure has the significant advantage that the master matrix is nonsymmetric but not complex.

2.1 Nonconforming Rectangular Element

The first finite element considered in the present study is the now well-known 12-degree-of-freedom nonconforming plate element. This element uses the three parameters w, $\partial w/\partial x$ and $\partial w/\partial y$ as generalized displacements at each corner and provides displacement continuity but not slope continuity between adjacent elements. The displacement vector of Eq. (9) for this element becomes

$$\{W\}^T = (w_{x1},w_{y1},w_1/a,w_{x2},\ldots,w_{x3},\ldots,w_{x4},\ldots) \tag{17}$$

where $w_x = \partial w/\partial x$, etc., and the subscripts 1 to 4 refer to the element corners shown in Fig. 1. The corresponding interpolation functions of Eq. (9) may be obtained from Ref. 2. Carrying out the calculations involved in Eq. (11) leads to the aerodynamic matrix given in Table 1.

2.2 Conforming Rectangular Element

The second finite element considered here is the relatively newer 16-degree-of-freedom conforming plate element.[3] This element uses one additional generalized displacement $\partial^2 w/\partial x\partial y$ at each corner and provides slope continuity as well as displacement continuity between adjacent elements. The displacement vector for this element is

$$\{W\}^T = (w_1/a,w_{x1},w_{y1},aw_{xy1},w_2/a,\ldots,w_3/a,\ldots,w_4/a,\ldots) \tag{18}$$

and the interpolation functions required in Eq. (9) are products of the one-dimensional Hermite polynomials given in Ref. 3. Again, carrying out the calculations of Eq. (11) for this element leads to the aerodynamic matrix given in Table 2.

2.3 Conforming Triangular Element

Finally, a triangular element is considered, so that problems with nonrectangular boundaries may be analyzed. The element chosen is a new 18-degree-of-freedom conforming model which exhibits a higher accuracy and faster convergence than any previously available representations. The initial formulation and some preliminary static results are presented in Ref. 4, and the general derivation is given in Refs. 5 and 6 along with extensive numerical verifications.

The element uses the six parameters w, $\partial w/\partial x$, $\partial w/\partial y$, $\partial^2 w/\partial x^2$, $\partial^2 w/\partial x\partial y$, and $\partial^2 w/\partial y^2$ as generalized displacements at each vertex. A brief outline of the element derivation follows. The displacement for the element is taken as a full quintic polynomial in two cartesian coordinates, and three constraints are placed on the polynomial to ensure that the slope normal to an edge $\partial w/\partial n$ varies cubically along each edge of the element. These three constraints are just sufficient to reduce the 21 terms in the quintic polynomial to 18 and hence make it compatible with the 18 generalized displacements for the element. In Ref. 6, the stiffness and mass matrices for the element are actually derived in terms of the polynomial coefficients in closed form. These matrices are generated in the computer and are then numerically transformed into corner displacement notation. The same procedure is followed to obtain the aerodynamic matrix. In the notation of Ref. 6, the elements of this aerodynamic matrix $[a]$ in terms of the polynomial coefficients are

$$a_{ij} = [2q/(M_\infty^2 - 1)^{1/2}][m_jF(m_i + m_j - 1,n_i + n_j)\cos\theta - n_jF(m_i + m_j,n_i + n_j - 1)\sin\theta]\ i,j = 1 \text{ to } 20 \tag{19}$$

Note that the air flow is assumed to be in the x direction in Fig. 1 of Ref. 6. Transforming to the corner displacements in the global coordinate system yields the required 18 × 18 aerodynamic matrix

$$[A_e] = [R]^T[T_2]^T[a][T_2][R] \tag{20}$$

All the calculations involved in Eqs. (19) and (20) are carried out directly in the computer, and only the rotation and transformation matrices need be written out explicitly. See Ref. 6 for details and definition of symbols used in Eqs. (19) and (20).

3. Results of Example Applications

Several example applications of the present method are presented in this Section. The method of calculation followed is to first set up the master aerodynamic-stiffness matrix of Eq. (13) for a particular assemblage of finite elements. The eigenvalues are then calculated for increasing values of the dynamic pressure parameter λ until first coalescence occurs. An iteration procedure is then introduced to calculate accurate values of λ_{cr} and k_{cr}.

3.1 Simply Supported Square Panel

The first application considered is that of a simply supported square panel, since it has an exact solution[8] and hence serves as a check on the method. Calculations are carried out with various assemblages of both rectangular elements discussed in Section 2. A typical element layout (4 × 4

Table 2 Aerodynamic matrix 25200 $(M_\infty^2 - 1)^{1/2}[A_e]/2qa^2b$ for conforming rectangular finite element[a]

−4680	936	−660	132	4680	−936	660	−132	1620	−324	−390	78	−1620	324	390	−78
−936	0	−132	0	936	−156	132	−22	324	−54	−78	13	−324	0	78	0
−660	132	−120	24	660	−132	120	−24	390	−78	−90	18	−390	78	90	−18
−132	0	−24	0	132	−22	24	−4	78	−13	−18	3	−78	0	18	0
−4680	−936	−660	−132	4680	936	660	132	1620	324	−390	−78	−1620	−324	390	78
936	156	132	22	−936	0	−132	0	−324	0	78	0	324	54	−78	−13
−660	−132	−120	−24	660	132	120	24	390	78	−90	−18	−390	−78	90	18
132	22	24	4	−132	0	−24	0	−78	0	18	0	78	13	−18	−3
−1620	−324	−390	−78	1620	324	390	78	4680	936	−660	−132	−4680	−936	660	132
324	54	78	13	−324	0	−78	0	−936	0	132	0	936	156	−132	−22
390	78	90	18	−390	−78	−90	−18	−660	−132	120	24	660	132	−120	−24
−78	−13	−18	−3	78	0	18	0	132	0	−24	0	−132	−22	24	4
−1620	324	−390	78	1620	−324	390	−78	4680	−936	−660	132	−4680	936	660	−132
−324	0	−78	0	324	−54	78	−13	936	−156	−132	22	−936	0	132	0
390	−78	90	−18	−390	78	−90	18	−660	1320	120	−24	660	−132	−120	24
78	0	18	0	−78	13	−18	3	−132	22	24	−4	132	0	−24	0

[a] Rows and columns 3, 4, 7, 8, 11, 12, 15, and 16 are to be divided by $s = a/b$.

grid) is shown in Fig. 2. Poisson's ratio is assumed to be 0.3.

It is of interest to consider first how well the finite elements approximate the in-vacuo vibration modes of the panel. Hence, numerical results are presented in Table 3 for the first two eigenvalues for $\lambda = 0$. It is interesting to note that the nonconforming element results converge towards the exact values from below, while the conforming results converge from above. Both elements give reasonable approximations for these eigenvalues, but the conforming results are far more accurate than the nonconforming ones.

When λ is increased from zero, the lowest two eigenvalues for this problem approach each other and coalescence to k_{cr}

Table 3 In-vacuo eigenvalues for simply supported square panel

Finite element grid	k_1		k_2	
	NRE[a]	CRE[b]	NRE	CRE
2 × 2	324.77	391.32	2592.0	2808.0
3 × 3	352.54	389.97	2171.0	2473.8
4 × 4	366.72	389.74	2247.2	2447.9
6 × 6	378.71	389.66	2335.5	2437.8
Exact values	389.636		2435.23	

[a] NRE non-conforming rectangular elements.
[b] CRE conforming rectangular elements.

at λ_{cr}. The plots of this coalescence are remarkably similar to those shown in Ref. 1 for the two-dimensional panel. Hence, they are not presented here, since they provide nothing new. The numerical results for coalescence as predicted by the various finite element assemblages are presented in Table 4 along with the number of degrees of freedom required for each calculation. It is seen that all the results appear to converge satisfactorily towards the exact solutions as the element gridworks are refined. The result from the 2 × 2 grid of nonconforming elements is an exception to this, but this result must be considered fortuitous in light of the free vibration results of Table 3. It is seen there that this element gridwork underpredicts k_1 and overpredicts k_2. These errors apparently compensate each other in such a way as to yield an unusually good coalescence prediction.

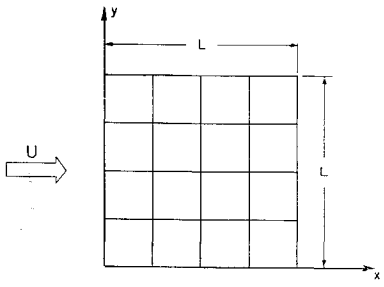

Fig. 2 Typical finite element layout for square panel (4 × 4 grid).

It may be seen from Table 4 that the convergence of the flutter predictions is not monotonic even for the conforming elements, whereas these elements do give monotonic convergence of the in-vacuo eigenvalues. This type of nonmonotonic convergence of the flutter solutions was already observed in Ref. 1 for the two-dimensional panel, so it is not surprising to find it here as well. Again it is clear from Table 4 that the conforming element results are far more accurate than the nonconforming ones. In fact, the 6 × 6 grid predictions for λ_{cr} and k_{cr} are only in error by 0.17 and 0.27%, respectively.

The actual rates of convergence of the finite element predictions are illustrated in Fig. 3 where the absolute relative errors are plotted vs n, the number of elements along an edge of the plate. The dashed lines with slopes of −2

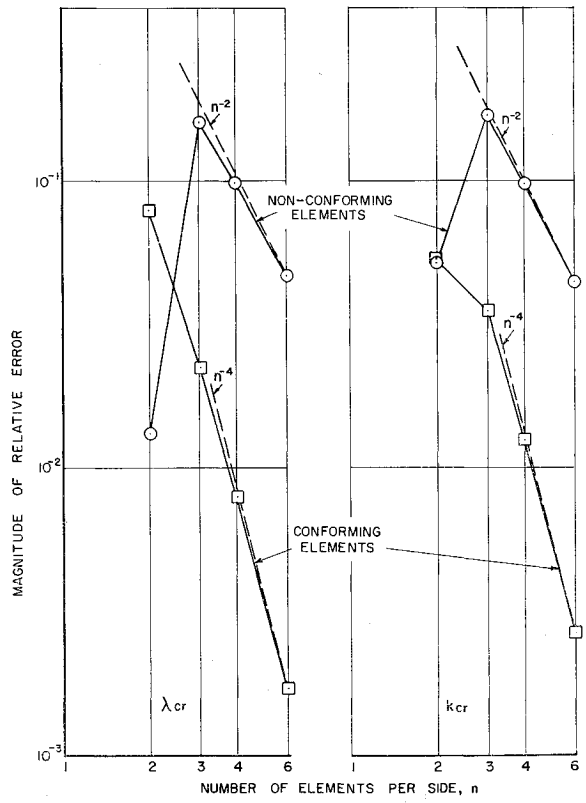

Fig. 3 Relative error of finite-element solutions for flutter of simply supported square panel.

Table 4 Eigenvalue coalescence results for simply supported square panel

Finite element grids	Total degrees of freedom	λ_{cr}	k_{cr}
	Nonconforming elements		
2 × 2	7	505.877	1751.91
3 × 3	20	430.527	1534.98
4 × 4	39	462.532	1668.04
6 × 6	51[a]	488.703	1766.24
Exact solution		512.651	1848.21
	Conforming elements		
2 × 2	16	552.835	1945.81
3 × 3	36	501.204	1782.79
4 × 4	64	508.609	1825.16
6 × 6	72[a]	511.786	1843.29
Exact solution		512.651	1848.21

[a] Using symmetry.

and −4 are included for reference. It is seen that the nonconforming element results appear to be approaching a slope of −2 for large values of n, whereas the conforming element results are approaching a slope of −4. This is significant in that these slopes are precisely the asymptotic slopes obtained with these respective elements in calculating the in-vacuo eigenvalues, as shown in Ref. 9. Hence, it is seen that the conforming elements provide faster convergence as well as smaller errors than the nonconforming elements.

3.2 Clamped Square Panel

The next application considered is that of a square clamped panel, a configuration for which no exact solution is available. Only the conforming rectangular elements are used for this example, since it is clear from the previous section that they give better results than the nonconforming ones. Poisson's ratio is again assumed to be 0.3. Some of the in-vacuo eigenvalue results are given in Table 5 along with the very accurate upper and lower bounds from Ref. 10. Again it is seen that the finite-element predictions of these eigenvalues are quite accurate and converge rapidly towards the "exact" values. However, the accuracy is not nearly as good as it was for the simply supported case (Table 3).

The eigenvalue coalescence results are given in Table 6 along with the number of degrees of freedom required in each case. These results appear to be converging very well for the more refined gridworks. In particular, the differences between the 5 × 5 and 6 × 6 grid predictions of λ_{cr} and k_{cr} are only 0.11 and 0.21%, respectively. Hence, it may be assumed that the 6 × 6 grid predictions are the "correct" values for most practical purposes. Note that the convergence again is not monotonic for the less refined element grids. The approximate values of λ_{cr} and k_{cr} given in the Table are due to Houbolt.[8] These values are surprisingly

Table 5 In-vacuo eigenvalues for clamped square panel using conforming rectangular elements

Finite element grid	k_1	k_2
2 × 2	1367.86	8684.3
3 × 3	1310.16	5626.4
4 × 4	1300.13	5480.9
5 × 5	1297.22	5427.0
6 × 6	1296.11	5406.7
Upper and lower bounds, Ref. 10	1294.96 1294.93	5386.7 5386.4

Table 6 Eigenvalue coalescence results for clamped square panel using conforming rectangular elements

Finite element grid	Total degrees of freedom	λ_{cr}	k_{cr}
2 × 2	4	1088.886	5026.08
3 × 3	16	817.934	4050.40
4 × 4	36	846.146	4244.35
5 × 5	64	849.492	4272.95
6 × 6	50[a]	850.418	4282.03
Approximation of Ref. 8		876.8	4077.

[a] Using symmetry.

good considering that they are based on a separated solution (which is fundamentally incorrect for a clamped panel) using only $1 - \cos 2\pi y/L$ for the y dependence of the panel deflection.

Finally, some calculations for $\lambda > \lambda_{cr}$ are carried out for this problem to give the flutter boundary as a function of the aerodynamic damping parameter g_a. The results obtained using the 6 × 6 grid of elements are given in Table 7 for values of λ up to 900. It appears that for this range of λ, k_R varies linearly and g_a varies quadratically with λ.

3.3 Cantilevered Delta Wings

The final application considered here is to the flutter of several cantilevered wings of delta planform. These examples serve to check out the method when using the triangular plate elements discussed in Sec. 2.3. The problem configuration and the two finite element assemblages used for the calculations are shown in Fig. 4. The only change from the previous applications to be noted is that now the air flows on both sides of the structure and the aerodynamic matrix is therefore doubled.

Table 7 Flutter boundary results for clamped square panel

λ	k_R	k_I
850.4	4282.	0
855.0	4292.	3.337
860.0	4304.	4.828
870.0	4326.	6.908
880.0	4349.	8.498
890.0	4373.	9.838
900.0	4396.	11.019

The calculations are carried out for the three sweepback angles Λ = 45, 60, and 70 degrees, and the results are compared with the experimental results given in Refs. 11 and 12. Results for the first three in-vacuo frequencies f_1, f_2, f_3 and for the flutter frequency f_f, neglecting aerodynamic damping, are presented in Table 8. Note that the number

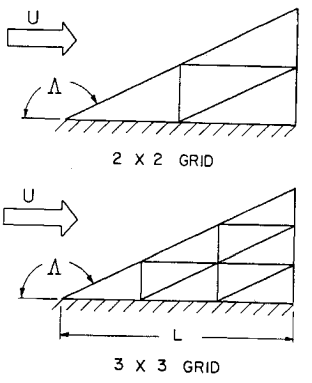

Fig. 4 Finite-element assemblages for cantilevered delta wings.

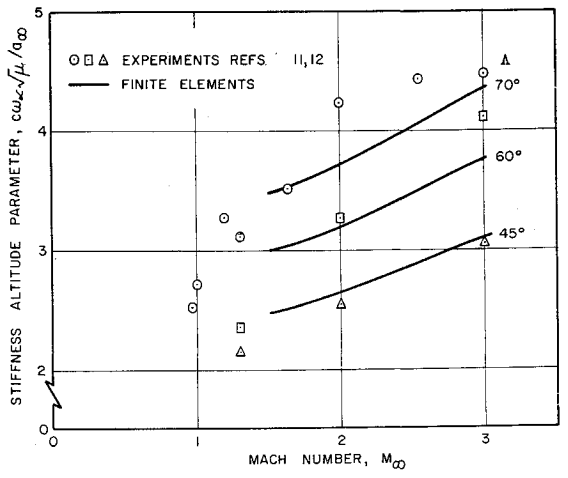

Fig. 5 Experimental and theoretical flutter boundaries for delta wings.

of degrees of freedom required for the 2 × 2 and 3 × 3 grid solutions were only 21 and 40, respectively. It is seen that the differences between the 2 × 2 and 3 × 3 grid predictions are very small. This is consistent with the experiences reported in Ref. 6, in that it was found there that extremely accurate results were always obtained by using only a few of these refined elements. In fact, it was also found that convergence rates approached n^{-6} for most of the static and dynamic problems treated. Hence, the 3 × 3 grid solutions may be considered to be the "correct" values for engineering purposes. The only possible exception to this may be the 70° delta where the predictions for f_2 and f_3 have changed appreciably. It may be noted that this case was checked by carrying out the calculations with a 4 × 4 grid of elements, and the first three frequencies obtained were 82.15, 194.7 and 349.4 cps. The small change in these frequencies indicates that the 3 × 3 grid solutions are indeed sufficiently accurate even for this case. The agreement between the predicted and experimental values is probably as good as can be expected, since the predictions are for an ideally clamped boundary, whereas the experiments (Refs. 11 and 12) used practical installations compatible with flutter testing.

The predicted values of λ_{cr} for the three delta wings are given in Table 9. Again the differences between the 2 × 2 and 3 × 3 grid predictions are quite small, and the 3 × 3 grid results may be taken as the "correct" ones. Using these results and neglecting aerodynamic damping, flutter boundaries as functions of Mach number are calculated and plotted in Fig. 5 along with the experimental points. The stiffness altitude parameter $c\omega_\alpha\mu^{1/2}/a_\infty$ as used here follows the

Table 8 Comparison of predicted with experimental frequencies for delta-wings

Freq., cps	f_1	f_2	f_3	f_f
		Λ = 45°		
2 × 2 grid	55.78	212.2	296.3	167.5
3 × 3 grid	55.72	211.9	295.2	167.6
Exp. Ref. 11	50	185	273	159
		Λ = 60°		
2 × 2 grid	76.40	224.9	394.6	194.6
3 × 3 grid	76.28	223.7	393.2	195.0
Exp. Ref. 11	67	200	342	180
		Λ = 70°		
2 × 2 grid	82.37	200.3	372.1	183.0
3 × 3 grid	82.22	195.1	355.7	182.1
Exp. Ref. 12	79	193	350	161

Table 9 Coalescence results for delta wings

Finite element grids	λ_{cr}		
	Λ = 45°	60°	70°
2 × 2	86.204	264.73	715.23
3 × 3	86.254	264.32	695.07

definition given in Ref. 11, except that ω_α is taken to be the second in-vacuo vibration frequency. The values for ω_α used to calculate the flutter boundaries are taken from the results of Table 8. It is seen that the agreement between the predictions and experiments is fairly good in all cases, but is especially good for the 45° delta. Some of the discrepancy for the 60° and 70° deltas may be due to the assumption of two dimensional aerodynamics, since these wings are of quite low aspect ratio.

4. Concluding Remarks

The application of the finite-element method to supersonic flutter problems has been presented. The present development employed two rectangular plate bending elements, one nonconforming and one conforming, and one triangular conforming element. It was found that the conforming rectangular element yielded higher accuracy and faster convergence than the nonconforming one. The triangular element was used to solve several delta wing problems, and the results compared well with experimental results.

The present method may be extended to solve previously unmanageable problems involving complicated boundary shapes and/or boundary conditions, in-plane stresses, nonuniform material, and so on.

References

[1] Olson, M. D., "Finite Elements Applied to Panel Flutter," *AIAA Journal*, Vol. 5, No. 12, Dec. 1967, pp. 2267–2270.

[2] Zienkiewicz, O. C., "The Finite Element Method in Structural and Continuum Mechanics," McGraw-Hill, London, 1967, Chaps. 7 and 11.

[3] Bogner, F. K., Fox, R. L., and Schmit, L. A., Jr., Addendum to "The Generation of Inter-Element Compatible Stiffness and Mass Matrices by the Use of Interpolation Formulas," *Matrix Methods in Structural Mechanics*, AFFDL-TR-66-80, 1966, Wright-Patterson Air Force Base, Ohio.

[4] Cowper, G. R. et al., "Formulation of a New Triangular Plate Bending Element," *Canadian Aeronautics and Space Institute Transactions*, Vol. 1, No. 2, Sept. 1968, pp. 86–90.

[5] Cowper, G. R. et al., "A High Precision Triangular Plate Bending Element," Aeronautical Rept. LR-514, National Research Council of Canada, Dec. 1968.

[6] Cowper, G. R. et al., "Static and Dynamic Applications of a High-Precision Triangular Plate Bending Element," *AIAA Journal*, Vol. 7, No. 10, Oct. 1969, pp. 1957–1965.

[7] Kariappa and Somashekar, B. R., "Application of Matrix Displacement Methods in the Study of Panel Flutter," *AIAA Journal*, Vol. 7, No. 1, Jan. 1969, pp. 50–53.

[8] Houbolt, J. C., "A Study of Several Aerothermoelastic Problems of Aircraft Structures in High Speed Flight," Ph.D. thesis, No. 2760, 1958, Swiss Federal Institute of Technology, Zurich, Switzerland.

[9] Lindberg, G. M., Olson, M. D., and Tulloch, H. A., "Closed Form, Finite Element Solutions for Plate Vibrations," Aeronautical Rept. LR-518, Feb. 1969, National Research Council of Canada.

[10] DeVito, L. et al., "Sul Calcolo degli Autovalori della Piastra Quadrata Incastrata Lungo il Bordo," *Rendiconti dell'Accademia Nazionale dei Lincei*, Ser. 8, Vol. 40, 1966, pp. 725–733.

[11] Tuovila, W. J. and McCarty, J. L., "Experimental Flutter Results for Cantilever-Wing Models," RM L55E11, June 14, 1955, NACA.

[12] Hanson, P. W. and Levey, G. M., "Experimental and Calculated Results of a Flutter Investigation of Some Very Low Aspect-Ratio Flat-Plate Surfaces at Mach Numbers from 0.62 to 3.00," TN D-2038, Oct. 1963, NASA.